Journal of Catalysis 427 (2023) 115099

Contents lists available at ScienceDirect

Journal of Catalysis

journal homepage: www.elsevier.com/locate/jcat

What factors determine activity of UiO-66 in H_2O_2-based oxidation of thioethers? The role of basic sites

Vasilii Yu. Evtushok, Kirill P. Larionov, Vladimir A. Lopatkin, Olga A. Stonkus, Oxana A. Kholdeeva *

Boreskov Institute of Catalysis, Lavrentieva Ave. 5, Novosibirsk 630090, Russia

ARTICLE INFO

Keywords:
Heterogeneous catalysis
Hydrogen peroxide
Liquid-phase oxidation
Metal–organic frameworks
Thioethers
Zirconium
UiO-66

ABSTRACT

Zr-based metal–organic frameworks (Zr-MOFs) have attracted significant attention as selective oxidation catalysts due to their stability in aqueous and oxidative media and high activity in H_2O_2 activation. Oxidation of thioethers with aqueous H_2O_2 over Zr-MOFs reveals extremely high selectivity toward the formation of sulfones even at low conversions. Herein, the main factors determining activity of Zr-MOF in the thioether oxidation have been investigated using zirconium terephthalate UiO-66 as a model catalyst and methyl phenyl sulfide (MPS) as a model substrate. Samples of UiO-66 differing in the particle size, number of defects, and composition have been synthesized. The particle size was evaluated based on high resolution transmission electron microscopy images. Thermogravimetric analysis (TGA), proton nuclear magnetic resonance spectroscopy (^{1}H NMR), and inductively coupled plasma atomic emission spectroscopy (ICP-OES) were employed for quantification of defects and determination of the composition of the UiO-66 samples. The number of basic sites was determined by liquid-phase adsorption of isobutyric acid. It was demonstrated that this characteristic depends on both the number of defects and specific composition of UiO-66 and can be affected by dehydration/hydration procedures. The number of basic sites turned out close to the number of terminal Zr–OH_2/OH groups in the Zr-MOF defects determined by combinations of ^{1}H NMR/TGA and ^{1}H NMR/ICP-OES, suggesting that the basic sites are represented by Zr-OH groups at open Zr sites. Kinetic studies implicated that catalytic activity of UiO–66 in MPS oxidation is proportional to the number of basic sites provided that the particle size of the Zr-MOF does not exceed 10–20 nm. Acid additives suppress both the thioether oxidation and H_2O_2 dismutation, pointing to the key role of basic Zr–OH groups in these two catalytic reactions.

1. Introduction

Metal–organic frameworks (MOFs) are porous coordination polymers composed of metal ions or clusters that are linked by polydentate organic ligands in a complex periodic reticular structure [1–3]. MOFs have extraordinary textural characteristics, vastly exceeding those of typical porous materials. In particular, their surface areas and pore volumes often lie in the range of 1000–3000 m^2/g and 1–3 cm^3/g, respectively [3,4]. Excellent porosity characteristics together with the possibility of introducing a variety of functionalities into a MOF structure give rise to intensified research in the fields of gas adsorption and separation [5–7], heat pumps [8,9], catalysis [10–15], sensing [16], drug delivery [17,18], and others.

MOFs represent a new type of heterogeneous catalysts as they feature high content of metal centers (20–40 wt%) and high porosity with an ordered structure that ensures easy access to the active sites provided that the size of reagents does not exceed the size of the MOF apertures [10–15]. They can serve not only as supports for active nanoparticles and metal complexes but may also possess intrinsic activity in acid–base and oxidation catalytic reactions [10,11,13,19–21]. The well-defined structure of spatially isolated active sites (metal nodes) facilitates their study at the molecular level and brings them closer to homogeneous catalysts [11,22].

Oxidation catalysis enables efficient insertion of oxygen into organic compounds and their transformation to valuable products and intermediates of organic synthesis [23–25]. One of the most attractive, green oxidants with high content (47%) of active oxygen is hydrogen peroxide, since the only by-product of oxidations with H_2O_2 is water [26,27]. Its widespread use is hindered by some economic factors and low reactivity; therefore, the development of new efficient catalysts for

* Corresponding author.
E-mail address: khold@catalysis.ru (O.A. Kholdeeva).

https://doi.org/10.1016/j.jcat.2023.115099
Received 16 March 2023; Received in revised form 13 August 2023; Accepted 18 August 2023
Available online 19 August 2023

its production in situ and activation is required [28]. Moreover, for selective oxidation of the majority of organic substrates, peroxide activation through a heterolytic pathway is preferable [23,24] in order to avoid generation of $^{\cdot}OH$ and $HO_2^{\cdot}$ radicals, which are detrimental to product selectivity, reproducibility, and oxidant utilization efficiency. So far, use of MOFs as catalysts for oxidations with H_2O_2 was lagged behind because of issues with MOF stability in the harsh environment of reaction mixtures containing H_2O_2 that has a strong hydrolyzing and coordinating abilities [29,30].

If we consider known MOFs from the view point of their potential use as catalysts for oxidation with H_2O_2, then it is worth highlighting the family of Zr-MOFs, the structure of which is based on Zr(IV) oxo-hydroxo clusters $\{Zr_6O_4(OH)_4\}^{12+}$ connected by polytopic carboxylate ligands [31–33]. Among them, zirconium terephthalate UiO–66 (the structure is shown in Fig. 1; UiO stands for University of Oslo) is the best known and deeply studied one. Zr-MOFs and especially UiO–66 are exceptionally stable at elevated temperatures, resistant to hydrolysis/solvolysis and do not degrade over a wide pH range [31].

These features of UiO-66 have brought about a keen interest in this material in the field of catalysis [34–37]. Recent studies have shown that Zr-MOFs exhibit catalytic activity in a range of liquid-phase oxidations with aqueous H_2O_2 [29,38–42]. The oxidation of S-compounds, thioethers and thiophens, in particular oxidative desulfurization (ODS), are among the most widely studied processes in which MOFs [43,44] and specifically Zr-MOFs [39–41,45–53] are used as catalysts. Meanwhile, catalytic activity of Zr-MOFs for the epoxidation of C = C bonds in alkenes [38,54,55] and α,β-unsaturated carbonyl compounds [39,40] has been also demonstrated. The results collected in a few works indicated that Zr-MOFs are capable of heterolytic activation of H_2O_2 followed by either electrophilic or nucleophilic oxygen transfer to organic substrate [38–40,52]. The oxidation mechanism depends on the nature of the organic substrate [39,40] and can be amended by the addition of a source of protons [38] or choice of solvent [39,52]. Despite significant progress in the perception of the H_2O_2-based oxidation catalysis on Zr-MOFs, there are still gaps in understanding of the key factors which govern the catalytic performance [29,40]. Filling these gaps would also expand our knowledge of the principles of H_2O_2/organic substrate activation on zirconium, which is currently an understudied area. For example, it is not yet clear why Zr-substituted polyoxometalates (Zr-POM) are highly active catalysts for epoxidation of various C = C bonds [56] while Zr-silicates [57] and Zr-MOFs [38] are not. Elucidation of the nature of active Zr sites in Zr-MOFs and elaboration of methods for their quantification would help in answering the key question–what factors affect the catalytic performance of Zr(IV)?

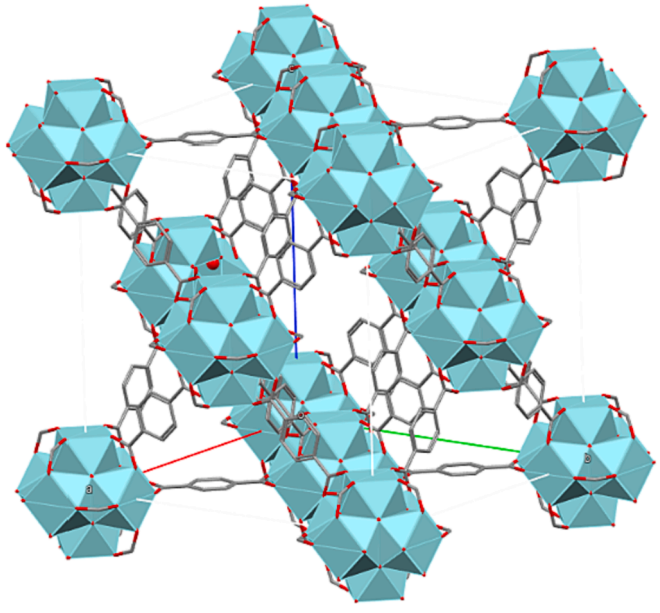

Fig. 1. Ideal structure of UiO-66. Edge terephthalate linkers are omitted for simplicity.

Zr-MOFs exhibit catalytic activity due to the properties of their nodes, Zr(IV) oxo-hydroxo clusters [31,58–61]. Such clusters themselves also reveal some activity in H_2O_2-based oxidations [39,61], but their organization into a regular porous structure of MOF improves drastically the catalytic performance. It is widely accepted that Zr-nodes provide catalytically active sites in the form of open Zr-sites, which can be either coordinatively unsaturated or terminated with labile groups [31,58,59,62]. The latter are commonly associated with a pair of Zr(H_2O)/ZrOH [63–65] (Fig. 2a) but special treatments can give other configurations [66]. Open Zr sites are considered to be active sites in both acid–base [58,59,63,67] and oxidation [29,39,52,59] catalysis due to Lewis acidity of coordinatively unsaturated Zr(IV) or Brønsted acid–base properties of terminal Zr(H_2O)/Zr(OH) groups. Yet, the catalytic performance of UiO-66 is often attributed to a dual acid/base character of the open sites [39,65,77].

Open Zr-sites can arise due to defects and/or a low-coordination mode of the nodes in some specific Zr-MOF structures [58,59]. Zr-MOFs with 12 linkers per node, specifically the most studied UiO-66, do not contain open Zr-sites in the ideal MOF structure (Fig. 1) [40,66,67]. The only way to get open Zr–sites in 12-coordinated Zr–MOFs is the generation of defects. Various approaches have been developed for defect engineering in Zr-MOFs, the most common being the use of carboxylic acid modulators during the solvothermal synthesis [68,69,70–71]. However, carboxylates can remain strongly bound with Zr-sites at thus generated missing linker defects (Fig. 2b). This means that the number of the missing linker defects can differ significantly from the number of catalytically active Zr-sites. Therefore, the use of defect quantification methods alone is not sufficient for a reliable determination of active sites in Zr-MOF, and it is necessary either to find out the exact composition of the MOF or determine the number of active Zr-sites directly.

Basic sites in Zr-MOFs can apparently play a significant role in catalysis [39,40,77,78]. However, at present, little is known about their structure and methods for their quantitative determination. The main candidates for the role of such sites were bridging μ^3-O [77] and terminal Zr-OH groups [65,72]. In our previous work, we suggested to employ liquid-phase adsorption of isobutyric acid (IBA) to determine the number of basic sites in Zr–MOFs [39,40]. Our interest was stimulated by the unusually high selectivity for sulfones observed in the oxidation of thioethers with H_2O_2 over Zr-MOFs [39,40]. Indeed, predomination of sulfones over sulfoxides, even at initial stages of the oxidation process, clearly points to nucleophilic activation of H_2O_2 [73,74], which usually requires basic conditions [75,76]. Preliminary results allowed us to suggest that basic sites in Zr-MOFs are most likely Zr-OH terminal groups located in defects (see Fig. 2a) [39,40]. However, no direct quantitative correlation that would link Zr-MOF activity with the number of basic sites was so far established, most likely, because other factors could also contribute to the observed activity. Given that the nature of basic sites in Zr-MOFs is a matter of discussion [65,77–79], studies devoted to its elucidation and resolving the problem of their quantification are challenging goals for both MOF chemistry and oxidation catalysis.

Catalytic activity of Zr-MOFs can be strongly affected by MOF adsorption properties [40], which are primarily defined by the nature of the organic linker and the specific MOF structure, and can be enhanced by increasing the defect concentration in MOF [80–83]. While Zr core provides catalytically active sites, the linker–substrate interactions tune the process efficiency [84]. Taking into account that studies of liquid-phase adsorption of organic compounds on MOFs are relatively scarce and rarely deal with typical substrates and products of selective oxidation [40,85–88], at the current state of knowledge, it is practically impossible to establish quantitative structure–activity relationships

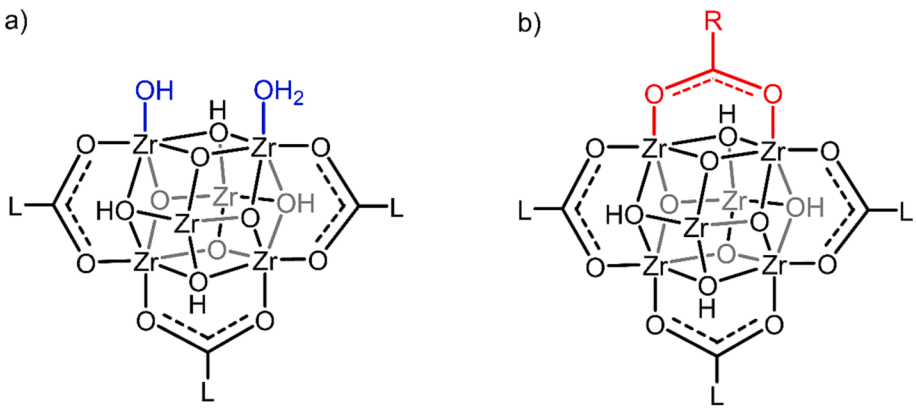

Fig. 2. Simplified representation of hydrated defect in Zr-node (L belongs to dicarboxylate linker): (a) open site with H_2O/OH terminal groups and (b) defect site capped with modulator carboxylate R-COO^-.

using Zr-MOFs of different structures [40]. This prompted us to concentrate only on the sole family member of Zr-MOFs, namely UiO-66, for a systematic investigation of the factors which may have impact on catalytic activity in the oxidation of S-compounds. Fortunately, to date, various methods have been described in the literature that make it possible to vary a certain characteristic of UiO-66 (for example, particle size, number of defects, or number of open sites) without altering the others.

It is well-known that accessibility of active sites for diffusion of reagents can critically affect activity of microporous catalysts, so mass transfer processes should be taken into account. UiO-66 has a pore aperture of 6 Å, which is sufficient for the penetration of a substituted aromatic ring inside the MOF pores. However, when the kinetic diameter of a substrate is close to the pore aperture, diffusion limitations may arise during the catalytic process, depending on the catalyst particle size and specific substrate reactivity. So far, mass transfer in Zr-MOFs has rarely been examined thoroughly in catalytic studies, especially in the liquid-phase [11,58,59,62,67]. Most of the works which addressed diffusion processes in UiO-66 dealt with small molecules and light linear alkanes with small kinetic diameter [89–92] and few works concerned gas-phase diffusion of organic molecules with the kinetic diameter close to the UiO-66 pore entrances [93,94]. Since kinetic trends can be strongly altered by internal diffusion limitations [95], to establish reliable quantitative correlations between the number of active sites in UiO-66 and its catalytic activity, a proper choice of the range of catalyst particle sizes and reaction conditions, which ensure the reaction proceeds in the kinetic regime, is required.

While our previous works concerned mainly selectivity issues in the Zr-MOF-catalyzed oxidations [38–40], the aim of the present work was to determine which factors affect activity of the catalysts and what is the role of basic sites among them. Using two series of UiO-66 samples differing in a variable parameter, either particle size or number of basic sites, we first systematically compared various methods employed so far for determination of terminal Zr(H_2O)/ZrOH groups, developed a reliable procedure for quantification of basic sites and, using a model substrate, methyl phenyl sulfide (MPS), determined the conditions under which catalytic oxidation proceeds in the kinetic regime, ensuring that MPS diffusion does not affect the catalytic activity. All these allowed us to verify the nature of basic sites in UiO-66 and find a correlation between their number and intrinsic catalytic activity of UiO-66 in the oxidation of thioethers with H_2O_2. Decomposition of H_2O_2 over UiO-66 was also investigated in the absence of organic substrate to clarify the role of basic sites in the possible side reaction–unproductive H_2O_2 degradation.

2. Experimental section

Materials. Acetonitrile (Panreac, HPLC grade) was dried and stored over activated 3 Å molecular sieves. Methyl phenyl sulfide (MPS, 99%), methyl phenyl sulfoxide (MPSO, 98%) and terephthalic acid (99%+) were purchased from Acros. All the other compounds were the best available reagent grade and were used without further purification. The concentration of hydrogen peroxide (ca. 30 % in water) was determined iodometrically prior to use.

Instrumentation. ^{1}H NMR spectra were recorded at 400.130 MHz on a Brüker AVANCE-400 spectrometer. Zr content was determined by ICP-OES using an Optima-430 DV instrument (PerkinElmer Inc.) ATR-FTIR spectra (4000–400 cm^{-1}, 32 scans, resolution 4 cm^{-1}) were obtained using a Cary 660 FTIR spectrometer (Agilent Technologies). Thermogravimetric analysis (TGA) and differential scanning calorimetry (DSC) were carried out in airflow (30 mL/min) using a NETZSCH STA 449C instrument. The sample weight was 10 mg in all experiments and the heating rate in TG experiment was 10 °C/min. Nitrogen adsorption measurements were carried out at 77 K using a Quantachrome NOVA 1200 instrument. The catalysts were activated in vacuum at 150 °C for 3 h before the measurements. Powder X-ray diffraction (PXRD) patterns were collected on a Shimadzu XRD 7000S diffractometer (Shimadzu, Kyoto, Japan) (CuKα radiation, graphite monochromator and Si as an external reference). Scanning electron microscopy (SEM) images were acquired by means of a JEOL JSM-6460 LV microscope. The particle morphology was studied by transmission electron microscopy (TEM) using a JEM-2010 (JEOL Ltd., Japan) and a JEM-2200FS (JEOL Ltd., Japan) electron microscopes operated at 200 kV. The samples were dispersed ultrasonically and deposited on TEM copper grids covered with a holey carbon film. GC analyses were performed using a gas chromatograph Tsvet-500 equipped with a flame ionization detector and a quartz capillary column (30 m × 0.25 mm) filled with BPX5.

Zr-MOF synthesis and characterization. UiO-66 samples were synthesized from $ZrCl_4$ or $ZrOCl_2{\cdot}8H_2O$ and H_2BDC by the solvothermal method using DMF as solvent and carboxylic acids as modulators, following the procedures reported by Taddei [96] and Gutov [97] (see Supporting Information (SI) for details). The structure of UiO-66 was confirmed by PXRD, FT-IR spectroscopy, and N_2 adsorption while average particle size for the UiO-66 samples was determined by SEM and TEM (Figures S1-S4). The number of defects in UiO-66 samples was assessed by TGA (see SI for calculations, Figure S5-S6); the temperature of ligand decomposition onset was determined at the foot of the largest peak (Figure S7). The composition of UiO-66 samples was evaluated following an approach reported by Limvorapitux et al. [52] based on the combination of ^{1}H NMR and ICP-OES and an adapted methodology suggested by Shearer et al. [69] using ^{1}H NMR and TGA. Before use,

samples were activated in vacuum at 150 °C for 5 h and stored in desiccator over P_2O_5.

Catalytic oxidations and kinetic experiments. Catalytic reactions were performed under vigorous stirring (500–600 rpm) in thermostated glass vessels. The reaction rate was independent on the rate of stirring, which excludes any effect of external diffusion limitation. MPS oxidation was initiated by addition of H_2O_2 (0.2 mmol) to a solution of MPS (0.2 mmol) in 2 mL of CH_3CN at 25 °C containing 4.4 mg of UiO-66. MPSO oxidations were carried out under the following conditions: 2 mg of UiO-66, $[H_2O_2] = 0.015$ M, [MPS] = 0.015 M, 4 mL CH_3CN, 25 °C. Samples of the reaction mixture were taken periodically, and MPS or MPSO consumption was determined by GC (with biphenyl as internal standard) after treatment of the reaction sample with PPh_3 to reduce the rest of H_2O_2. Initial rates were determined from experimental kinetic curves as d[MPS]/dt (or d[MPSO]/dt) at t = 0 by using a Cubic spline interpolation. Each experiment was reproduced 2—3 times.

Hydrogen peroxide decomposition study. Decomposition of H_2O_2 (0.2 M) was studied in the absence of an organic substrate at 50 °C in CH_3CN (2 mL) in the presence of UiO-66 (10 mg). Aliquots of 0.1 mL were taken during the reaction course, and H_2O_2 concentration was determined by titration with $KMnO_4$ (see SI for details). A maximum of 7 aliquots were taken during one kinetic experiment. At least two parallel experiments were carried out.

IBA adsorption studies. For evaluation of the number of basic sites in UiO-66 samples, the method suggested by Carniti et al. [98] was adapted with significant modifications [39]. A detailed description of the procedure is given in the SI. Adsorption studies were performed with 10 mg of UiO-66 preliminary activated (150 °C in vacuum) and then exposed to air for ca. 10 min in an open glass vessel before addition of 2 mL of *n*-hexane. A solution of isobutyric acid (IBA, 0.1 M in *n*-hexane) was added by 20 μL portions to the UiO-66 suspension in *n*-hexane, the suspension was stirred vigorously for 10 min and then the catalyst was allowed to settle and the IBA concentration in the solution was determined by GC (BPX-5) using *n*-decane as internal standard.

3. Results and discussion

3.1. Catalyst synthesis and general characterization

Two series of UiO-66 samples have been synthesized to fulfil the objectives of this work. The first series with variable particle size (VS-1 – VS-4) was prepared to answer the question of whether mass transfer limits the MPS oxidation rate over UiO-66 under typical reaction conditions and what particle size guarantees the kinetic regime of the reaction. The second series of samples with variable number of basic sites (VB-1 – VB-3) was prepared to elucidate the nature of basic sites in UiO-66 and their role in H_2O_2 activation and oxidation of organic S-compounds. Within each series, it was necessary to vary only one parameter of UiO-66 while fixing the others. Specifically, in the first series, we had to vary the particle size, keeping the total number of defects and number of basic sites fixed, in order to exclude the influence of any other factors, except for the mass transport. On the other hand, for investigation of the issues related to the intrinsic catalytic activity (the second series), we needed highly defective samples to get a maximum possible range in the number of basic sites with a similar number of defects. Moreover, the samples of the second series had to have a similar, critical particle size which enables to avoid the influence of diffusion limitation.

All the samples of UiO-66 were prepared by the solvothermal synthesis in DMF solvent using carboxylic acids as modulators (a detailed description of the synthesis protocols can be found in the SI). After synthesis, the samples were subjected to the same activation procedure in vacuum at 150 °C for 5 h. The main characteristics of the UiO-66 samples are presented in Table 1.

A set of samples VS-1 – VS-4 with different average particle sizes and similar high number of defects was prepared using $ZrCl_4$ as Zr-source by the method described by Taddei et al [96]. In this method, the variation of the particle size with similar other parameters is achieved by varying the aging time of the reaction mixture before heating while the mixture composition remains constant.

Table 1
The textural characteristics (N_2 adsorption), average particle size (TEM), and the number of linkers per node (TGA) of UiO-66 samples.

Sample	S_{BET}, m^2/g	$S_{external}$, m^2/g	V_{total}, cm^3/g	Average particle size, nm	Number of linkers per node
VS-1	1123	119	0.66	10 ± 4	9.4
VS-2	1181	113	0.71	18 ± 6	9.2
VS-3	1209	105	0.78	27 ± 7	9.5
VS-4	1250	85	0.68	30 ± 14 and 111 ± 21[a]	9.3
VB-1	1273	320	0.84	10 ± 2	9.2
VB-2	1176	362	0.74	9 ± 2	8.6
VB-3	1302	381	0.94	10 ± 2	7.9

[a] Bimodal distribution with predomination of peak centered at ca. 110 nm.

In the second series, highly defective samples with nanosized (<15 nm) particles, VB-1 and VB–2, were synthesized using $ZrOCl_2$ as Zr-source in the presence of acetic and formic acid as modulator, respectively, following the methodology reported by Gutov et al [97]. In addition, a sample with the highest content of H_2O/OH terminal groups, VB-3, was obtained by a slight modification of this procedure. We have noticed that, if the reaction mixture was cooled and left for a long time (1–2 weeks) after the synthesis, the acetate capping defects were gradually replaced by H_2O/OH pairs, as confirmed by TGA, ^{1}H NMR and ICP-OES (vide infra).

The synthesis methods used in this work were proved to be well reproducible and yielded samples having characteristics similar to those described in the literature. Most of the procedures had also advantage of the good yield of UiO-66 per volume unit of the reaction mixture. This was especially important for studying catalytic activity because it allowed us to work using a single batch of each UiO-66 sample.

The textural characteristics of the samples determined by N_2 adsorption were typical of UiO-66 (Table 1). In agreement with the literature [62,69], the surface area and pore volume increased slightly with increasing number of MOF defects. Also, as expected, decreasing the particle size of the UiO-66 samples led to a larger external surface area determined by the t-plot method.

The samples were examined by TEM and SEM techniques (representative TEM and SEM images are given in Fig. 3, S1 and S2). It is important to note that, only from TEM images, the size of UiO-66 particles can be accurately estimated if they are smaller than 100 nm. Particles in such samples are often poorly faceted and clumped into aggregates, which prevents accurate determination of their average size using SEM images, while TEM images clearly show the boundaries of individual crystallites. Fig. 3 shows TEM images of VS-1, VS-2, VS-3, and VS-4 samples acquired at the same magnification along with corresponding particle size distributions in the insets. For non-spherical or irregularly shaped particles, the projected area diameter was used as the particle size. As one can judge from Fig. 3, the average particle size increased in the order VS-1 < VS-2 < VS-3 < VS-4. In the VS-4 sample, a bimodal particle size distribution was noted, with predomination of the larger particles of ca. 110 nm.

All obtained PXRD spectra correspond to the one simulated for UiO-66 (see Figure S3). However, the PXRD patterns of the set of samples VS-1 – VS-4 reveal a gradual broadening of the peaks with decreasing the average particle size, which was an expected trend [99] (Fig. 4).

The IR spectra of all the UiO-66 samples (Figure S4) coincide with the spectra reported in the literature [31,100].

3.2. Defect concentration and composition of UiO-66 samples

The number of defects in Zr-MOFs, including UiO-66, are commonly

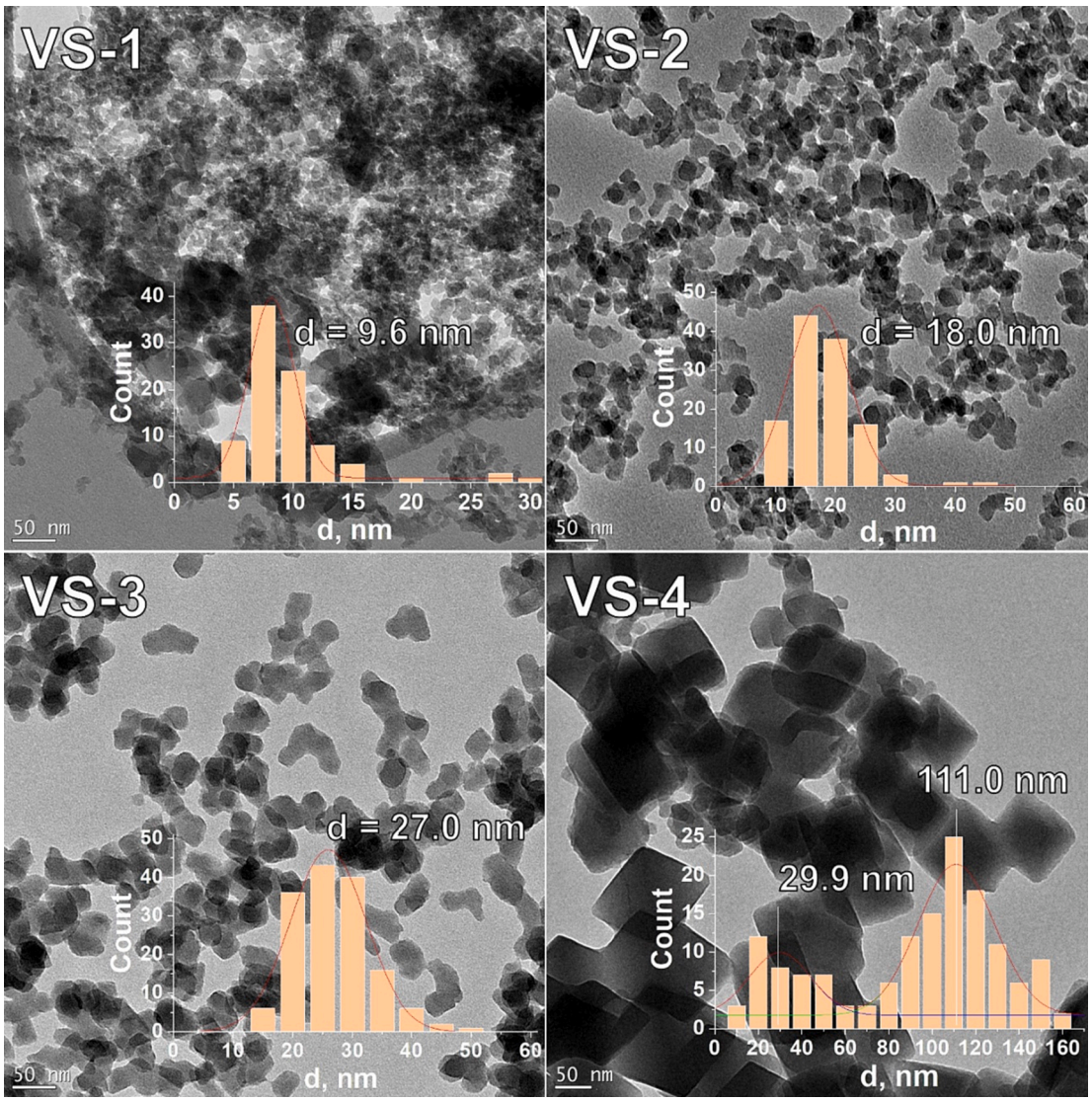

Fig. 3. TEM images of UiO-66 samples VS-1 – VS-4 presented at the same scale; the particle size distributions are shown in the insets.

determined by the TGA method [31,58,59]. The analysis of the literature shows that this method is sufficiently reliable, despite some possible problems associated with its use. The main sources of errors can be the presence of amorphous ZrO_2 phase or unreacted ligand remained in the MOF pores, incomplete combustion of ligands, as well as the presence of a large number of defects of the missing cluster type. In general, though, TGA has been shown to give accurate and consistent results when used carefully [31,58].

The data on the defect concentration in the UiO-66 samples determined by the TGA method are shown in Table 1. In general, the defect concentration in UiO-66 samples prepared in this work agreed with the literature data reported for UiO-66 obtained by the same methods. It is important to emphasize that the number of defects in samples VS–1 – VS-4 was quite high and similar (ca. 9.4 linker per node). Since this series of samples was employed to investigate the impact of mass transfer in the thioether oxidation, a comparable number of defects was crucial to limit the effect that could arise from its variation.

As we mentioned in the Introduction, knowledge of the number of defects is often insufficient to understand the catalytic properties of Zr-MOFs. Recent catalytic studies suggested that active sites in Zr-MOFs are represented by coordinatively unsaturated Zr–sites or Zr-sites terminated by labile H_2O/OH pair [58,59,62,65,77]. However, besides such catalytically active Zr-sites, catalytically inert Zr-sites capped by modulator acid carboxylates may also be present in the defects [52,67]. Thus, the quantification of active sites is possible either using a direct determination method or by establishing the exact composition of a fully hydrated Zr–MOF corresponding to the formula $Zr_6(OH)_4O_4(Ligand)_x(Modulator)_y(H_2O/OH)_z$ or a fully dehydrated one with the formula $Zr_6O_{6+z/2}(Ligand)_x(Modulator)_y$.

Methods for direct determination of catalytically active Zr-sites are being actively developed and currently they are represented by FTIR spectroscopy with probe molecules [68,79,101], solid state NMR with probe molecules [102,103], and potentiometric titration [104,105]. These methods rely on the acid–base properties of the H_2O/OH terminal groups or on the Lewis acidity of the coordinatively unsaturated Zr-sites. Yet, accurate quantification of catalytic Zr–sites by FTIR with adsorption of probe molecules requires knowledge of the exact absorption coefficients, the determination of which is a difficult task without additional confirmatory methods. In turn, solid state NMR with probe molecules, by its concept, can be used for the quantification of catalytically active centers, but there are only data on the quantification of defects in general [102,103]. So far, the data acquired by potentiometric titration have not yet been strictly confirmed by comparison with other methods. Taking all these into account, we resort to quantification of H_2O/OH terminal groups by calculating their number on the basis of the exact composition of our UiO-66 samples. The composition was

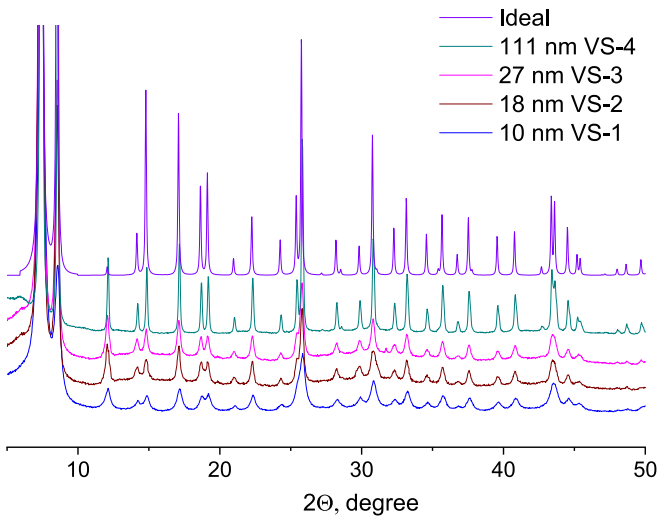

Fig. 4. PXRD spectra of UiO-66 samples with varied average particle size.

determined using two different approaches. Detailed calculations along with comments for both methods are given in the SI. All the UiO-66 samples were washed with DMF and acetone after the synthesis and then activated in vacuum at 150 °C, so their composition could not be affected by ligand and acid modulator residues in the pores (as was earlier demonstrated by Shearer et al. [106]).

In the first approach, solutions of the UiO-66 samples digested in the mixture of DMSO-d_6/HF were studied using a combination of ^{1}H NMR and ICP-OES. This method was described in detail by Limvorapitux et al. [52]. ^{1}H NMR spectra of a digested UiO-66 sample with an internal standard give information on the amount of BDC ligand and modulator acid in the MOF. However, to determine the composition, it is also necessary to know the amount of Zr in the same UiO-66 solution, which is provided by ICP-OES.

Another approach for the composition evaluation was proposed by Shearer et al [69] and further developed by Sannes et al [107]. It is based on a blend of TGA and ^{1}H NMR of a digested UiO-66 solution. In this method, an internal standard is not necessary for ^{1}H NMR measurements, since information about the ratio of zirconium to the organic part is provided by TGA. However, in our work, we used for ^{1}H NMR analyses the same solutions of UiO-66 digested in a mixture of DMSO-d_6/HF. Firstly, in this way we exclude the difference in determined terminal H_2O/OH groups between the methods associated with the errors in the preparation of different digested solutions, and secondly, the digestion procedure using NaOD described in the original work [69] leads to the residual precipitate of $ZrO_x(OH)_y$ which is inconvenient to separate.

Meanwhile, we have found that the number of terminal groups in various UiO-66 samples calculated based on the hydrated UiO-66 formula obtained by the two methods is sensitive to the accuracy of the corresponding analytical technique. In the case of the combination of ^{1}H NMR + ICP-OES, there is a very high sensitivity with respect to the amount of Zr in the solution of digested MOF. At a typical Zr concentration in a digested sample solution of 70 ppm, an error of 2% leads to an uncertainty in the number of the terminal groups of ± 500 μmol/g. Such error of the ICP-OES method is quite typical, especially for Zr [108], which is difficult to convert to a soluble form. Therefore, the use of this method is associated with the probability of a significant error in the calculation of the number of H_2O/OH terminal groups in UiO–66.

The combination of ^{1}H NMR + TGA shows a more tolerable sensitivity. An error in the normalized weight of ± 2% leads to an uncertainty in the amount of H_2O/OH terminal groups of ± 200 μmol/g. However, an additional problem may be a somewhat arbitrary choice of the ligand decomposition onset temperature in TGA curves. So far, little attention was devoted to this matter in the literature. We decided to rely on the differential scanning calorimetry and determined the decomposition onset temperature at the foot of the largest peak.

Data on the total defect concentration (open sites + modulator carboxylate capped sites) determined by TGA and the number of terminal H_2O/OH groups of the UiO-66 samples acquired by the two methods are shown in Table 2, along with data on the number of basic sites and catalytic activity of the UiO-66 samples expressed in terms of turnover frequency (TOF), which will be discussed in the following sections. As we can see, the number of terminal H_2O/OH groups calculated from the composition of UiO-66 samples is, in general, significantly less than the total number of defects determined by TGA. This discrepancy is consistent with the assumption that not every defect is related to a pair of H_2O/OH groups.

3.3. Determination of basic sites through liquid-phase adsorption of isobutyric acid

In our previous work, we found that IBA can be strongly adsorbed onto various Zr-MOFs [39,40]. We assumed the existence of basic sites and also linked the presence of these basic sites to the unusually high selectivity for sulfone in the oxidation of thioethers with H_2O_2 over Zr-MOFs, which is characteristic of nucleophilic oxidation [39,40]. Another indication of the nucleophilic activation of H_2O_2 was an ability of Zr-MOFs to catalyze the epoxidation of electron-poor C = C bonds, even in competition with electron-rich ones (e.g., in carvone) [40]. We suggested that namely basic sites are responsible for the nucleophilic character of active peroxo species formed upon the interaction of Zr-MOFs with H_2O_2.

While studying systematically IBA adsorption on UiO-66, we have noticed that the character of the IBA adsorption isotherm on Zr-MOFs strongly depends on the storage time after MOF activation (see SI for details, Figure S10). When IBA is adsorbed onto Zr-MOF immediately after activation, irreversible adsorption is effectively non-existent and only reversible adsorption occurs (Fig. 5). However, the isotherm of samples exposed to air, revealed also a portion corresponding to irreversible adsorption (Fig. 5). The maximum value of the irreversible adsorption could be reached after exposure in air for 10 min at relative humidity of 50–60% (see SI for details).

If we suggest that the basic sites are the terminal Zr-OH groups, we can rationalize these findings in terms of reversible dehydration with removal of terminal H_2O/OH groups in Zr-MOF during activation and hydration during storage in air (Scheme 1). Such behavior of the terminal groups in MOF defects is well documented in the literature [62–64,109,110]. We may assume that the maximum irreversible adsorption corresponds to the regeneration of all terminal H_2O/OH groups that had been removed during the activation. The subsequent decrease in the IBA adsorption value (Figure S10) is, probably caused by physisorption of water inside the pores of Zr-MOF [111,112]. During the liquid-phase IBA adsorption there should be a displacement of water from the pores into the solvent, and thus the water adsorbed in UiO-66 will negatively affect adsorption of IBA due to immiscibility with *n*-hexane. Apparently, the low water vapor pressure in the desiccator is sufficient for the slow regeneration of H_2O/OH groups, but not sufficient for the subsequent physisorption of a significant amount of water. Hence, for the most accurate determination of the number of basic sites by IBA liquid-phase adsorption, it is necessary to keep UiO-66 samples after activation in a desiccator over P_2O_5, at least, for one week before adsorption measurements. Alternatively, samples can be exposed to air for ca. 10 min. for faster hydration. However, in this case, the results may vary slightly depending on the air humidity, so preliminary experiments with different exposure times are required, as shown in Figure S10.

Previously, we have found a rather good match between the number of basic groups determined by IBA adsorption and the number of ZrOH groups estimated by TGA for UiO-66 and UiO-67 samples prepared without modulators and thus having relatively low number of defects

Table 2
Total defect concentration, number of terminal H_2O/OH groups, number of basic sites in UiO-66 samples, and turnover frequencies in MPS oxidation.

Sample	Total defect concentration by TGA,[a] μmol/g	Terminal H_2O/OH groups by ^1H NMR/TGA, μmol/g	Terminal H_2O/OH groups by ^1H NMR/ICP-OES, μmol/g	Basic sites by IBA liquid-phase adsorption, μmol/g	Turnover frequency,[b] s^{-1}
VS-1	1800	600	500	650	0.072
VS-2	1900	650	700	610	0.07
VS-3	1760	710	730	690	0.057
VS-4	1840	700	550	670	0.028
VB-1	1900	880	400	1060	0.058
VB-2	2200	1190	1080	1280	0.053
VB-3	2600	1520	1240	2010	0.05
UiO-66[a]	750	n.d.	n.d.	700	0.05
UiO-67[a]	1300	n.d.	n.d.	1150	n.d.

[a] TGA and IBA adsorption data for UiO-66 and UiO-67 synthesized without modulators (taken from Ref 45). [b] TOF = initial rate of substrate consumption (mol of substrate / s) / number of basic sites (mol). Reaction conditions: [MPS] = 0.1 M, [H_2O_2] = 0.1 M, UiO-66 catalyst 4.4 mg, 25 °C, 2 mL CH_3CN.

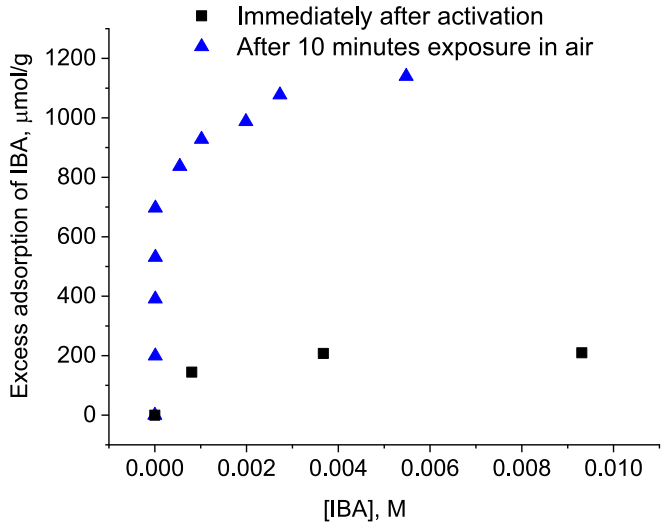

Fig. 5. Isotherms of IBA adsorption on UiO-66 (sample VS-3, *n*-hexane, 25 °C) measured immediately after activation (150 °C in vacuum) and after exposure in air for 10 min.

(1–2 missing linkers) [39]. However, for the highly defective UiO-66 samples prepared in this work, the situation was expected to be different because a part of defect sites could be capped by modulator carboxylates. Therefore, all the UiO-66 samples prepared in this work were thoroughly investigated by the liquid-phase adsorption of IBA. Data on the number of basic sites are collected in Table 2. The previously acquired data for lower defective UiO-66 and UiO-67 are also given for the sake of comparison.

As one can judge from Table 2, the number of basic sites for the UiO-66 samples synthesized with modulators corresponds well to the number of terminal H_2O/OH groups determined by the ^1H NMR/TGA combination, while the method based on the combination of ^1H NMR/ICP-OES gives significant discrepancies for some samples. As was mentioned above, this is, most likely, due to the strong sensitivity of the latter method to the amount of Zr determined by ICP-OES. Note that the number of terminal ZrOH groups in Zr-MOF is often significantly less than the number of μ^3–O groups, the number of which can be estimated based on the formula $Zr_6(OH)_4O_4(Ligand)_x(Modulator)_y(H_2O/OH)_z$ and lies in range of 2400–2700 μmol/g. The observed dependence of the number of basic sites on the sample activation and storage also strongly supports the assumption that the basic sites determined by the IBA adsorption are represented by the terminal ZrOH groups located at the open sites of the MOF. Given that ZrOH groups in the open sites coexist with Zr(H_2O) groups (Fig. 2a), the IBA adsorption may also allow estimation of Brønsted acid sites represented by the terminal Zr(H_2O) groups.

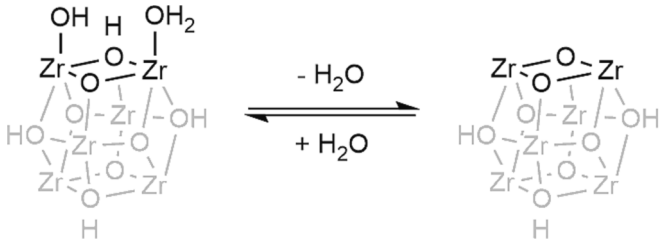

Scheme 1. Reversible removal of terminal H_2O/OH groups in Zr-MOFs during activation at elevated temperatures in vacuum.

3.4. Diffusion limitations in MPS oxidation

It is well-known that investigation of structure–activity relationships in heterogeneous catalysis should be carried out in the kinetic regime of the catalyst operation or with consideration of diffusion limitations, otherwise, the reaction rate can be not directly proportional to the number of active sites, leading to incorrect conclusions [11,95].

One of the methods for revealing the presence of diffusion limitations in heterogeneous catalysis is measuring the activation energy of the catalytic reaction in a wide temperature range [95]. In this case, different catalytic reaction regimes with different activation energies may be observed on the Arrhenius plot. Normally, the activation energies, E_a, of catalytic oxidation reactions with H_2O_2 (>10 kcal/mol) [56,113,114] are significantly higher than typical diffusion activation energies observed for meso- and macroporous catalysts (4–6 kcal/mol) [95]. Therefore, alterations in the observed activation energy with increasing temperature or its too low value usually indicate the presence of diffusion limitations. However, for microporous catalysts such as UiO-66, the activation energy of diffusion can be much higher (6–10 kcal/mol) because of the passage through small pore apertures and tetrahedral cages that tightly confine the guest molecules [115,116]. This makes problematic conclusions about the presence (or absence) of diffusion limitations on the basis of the values of Arrhenius activation energies for the oxidation of highly reactive substrates, such as thioethers and sulfoxides (E_a of ca. 10 kcal/mol have been found for both MPS and MPSO oxidations over UiO-66, Scheme 2) [39].

Therefore, we resorted to direct determination of the dependence of

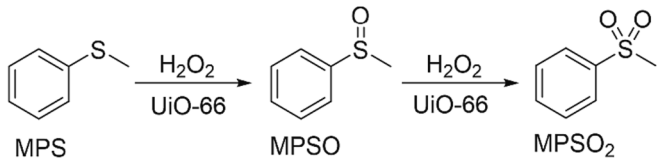

Scheme 2. MPS oxidation with H_2O_2 over UiO-66.

the initial rate of MPS oxidation on the average particle size of UiO-66, since this is the most reliable way to reveal internal diffusion limitations [95]. For this purpose, we used the series of samples VS-1 – VS-4 prepared using the same modulator (AcOH) and Zr-source ($ZrCl_4$) and having different average particle size (see Table 1) but similar total defect concentration and number of basic sites (Table 2). All of the samples examined were highly defective, which is important because the high defect concentration can probably improve diffusion of the organic substrate within the MOF crystallites.

The experimental dependence of the initial reaction rate on the average catalyst particle size is shown in Fig. 6. From this dependence (and also from TOF values given in Table 2), we can conclude that the oxidation of MPS with H_2O_2 over UiO-66 is definitely a diffusion-limited process even if highly defective UiO–66 samples are employed. By fitting Eq S22 (see SI), which describes the relationship between the reaction rate and average particle size through the Thiele modulus [95], we were able to extrapolate the experimental dependence to even smaller particle sizes (Fig. 6). Note that the reaction rate for sample VS-4 is slightly higher than the one predicted by the Eq S22 fit. This might be attributed to the presence of a fraction of particles with a smaller average size (see Table 1). The obtained fit shows that as the particle size reaches ca. 10 nm, the dependence of the reaction rate on the size of UiO–66 crystallites becomes weak, indicating that the catalyst starts to operate in the kinetic regime of the MPS oxidation. It is likely that this boundary of ca. 10 nm is relevant for substrates that are similar in their kinetic diameter to MPS. On the other hand, for a less reactive substrate, larger catalyst particles may ensure the kinetic regime.

Previously, Limvorapitux et al. have found that the observed rates of both MPS and MPSO oxidation over UiO-66 increased with enlarging the number of open sites, which had been determined based on the exact composition of the MOF [52], However, the rates were not proportional to the number of the open sites determined by ^{1}H NMR/ICP-OES, and the authors suggested that the lack of the direct correlation was due to the different local steric environment of the open sites in different UiO-66 samples. However, given that the average particle size of the UiO-66 samples they used was 150–200 nm, at the current state of knowledge, we may conclude that their activity could be significantly controlled by diffusion within the MOF crystallites.

3.5. Role of basic sites in MPS catalytic oxidation

Since diffusion limitations in the oxidation of MPS over UiO-66 are minimal while using catalysts with small particles, to study the relation between the number of basic sites and catalytic activity, we used the series of samples VB-1 – VB-3 with the average crystallite size of ca. 10 nm and high number of defects. For these samples, the MPS oxidation rate turned out proportional to the number of basic sites estimated by IBA adsorption (Fig. 7). Sample VS–1, which also has the particle size of ca. 10 nm, fits well with this correlation, indicating that the source of Zr used for the UiO-66 synthesis is not critical for catalytic activity. Fig. 7 also shows the initial reaction rates for UiO–66 samples VS-2 – VS-4, which have similar amounts of basic sites, but differ in the particle size. While sample VS-2 (18 nm) still fits well with the correlation, then VS-3 (27 nm) and especially VS-4 (ca. 30 and 110 nm) fall out of it, clearly reflecting diffusion limitations. This is also manifested by the TOF values given in Table 2, which are rather similar for samples within series VB-1 – VB-3 but decrease significantly on going from samples VS-1 – VS-2 to sample VS–4. Interestingly, the low defective UiO-66 sample prepared without modulator [39] revealed just slightly lower activity than it would be expected based on the plot depicted in Fig. 7, which indicates that the small particle size of this sample (<20 nm) compensates partially the low defect concentration which could hinder diffusion.

The type of acid modulator capping partially the defects does not seem to affect significantly the observed activity. Sample VB-2 prepared with formic acid (the other samples were prepared using acetic acid) showed the initial rate value that fits well the linear plot (Fig. 7).

In principle, the dependence of the catalytic activity of UiO-66 in MPS oxidation on the number of basic sites shown in Fig. 7 does not in itself prove the key role of basic sites in the activation of hydrogen peroxide and thioether oxidation to sulfoxide and sulfone. Firstly, each basic site is adjacent to acidic sites of terminal Zr-OH_2 and bridging Zr-(OH)-Zr (see Scheme 1), and secondly, their basic nature may be irrelevant for the catalysis. To verify whether the basic character of the terminal Zr-OH groups is crucial to accomplish the thioether oxidation to sulfone, we examined the effect of acid additives on the rates of MPS and MPSO oxidation.

Kinetic experiments were carried out using sample VB-1 in the presence of various amounts of strong mineral acid $HClO_4$. For MPSO oxidation, lower concentrations of the reactants were used because the MPSO oxidation is an order of magnitude faster relative to the MPS oxidation. The catalytic activity expressed in TOF values decreased drastically when acid was added to the reaction mixture up to 1 equiv. with respect to the basic sites (Fig. 8a). When more acid was added (>1 equiv.), oppositely an increase in the oxidation rate was observed and, starting from a certain amount of acid, sulfoxide began to dominate over sulfone among the oxidation products, indicating change in the

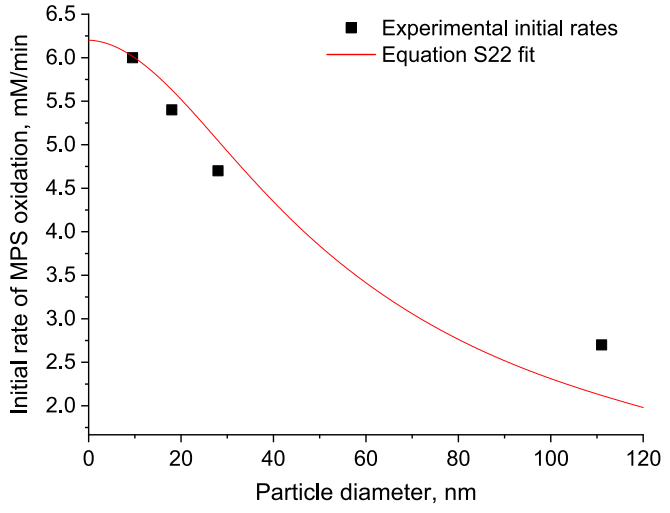

Fig. 6. Initial rates of MPS oxidation over UiO-66 samples VS-1 – VS–4 versus average catalyst particle size along with Eq S22 fit.

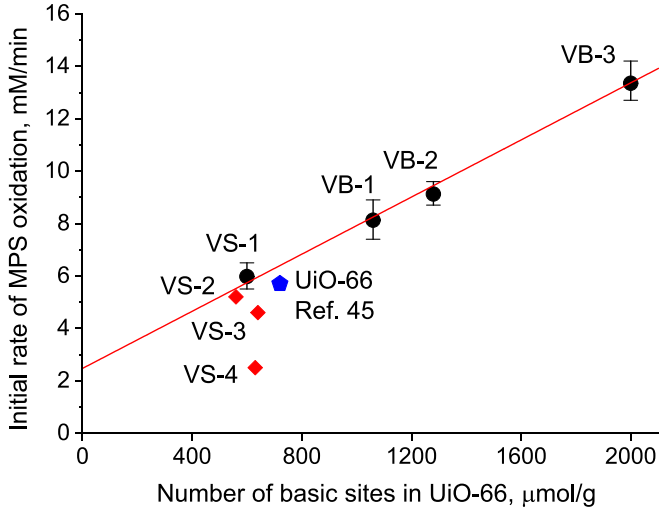

Fig. 7. Initial rate of MPS oxidation versus the number of basic sites in UiO-66 samples. Reaction conditions: [MPS] = 0.1 M, [H_2O_2] = 0.1 M, catalyst UiO-66 4 mg, 25 °C, 2 mL CH_3CN.

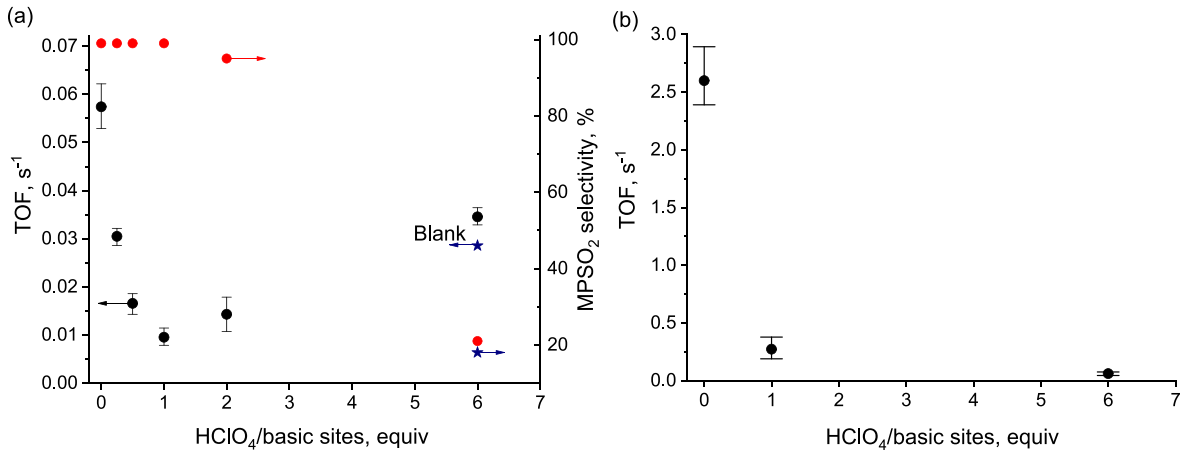

Fig. 8. The effect of $HClO_4$ additives on (a) TOF (●) and selectivity for $MPSO_2$ (●) in MPS oxidation and (b) TOF in MPSO oxidation. Reaction conditions: (a) [MPS] = 0.1 M, [H_2O_2] = 0.1 M, catalyst VB-1 4 mg (total amount of basic sites 1060 μmol/g), 25 °C, 2 mL CH_3CN; (b) [MPSO] = 0.015 M, [H_2O_2] = 0.015 M, VB–1 2 mg, 25 °C, 4 mL CH_3CN.

oxidation mechanism from nucleophilic to electrophilic one [39]. However, this rate increase upon the addition of high amounts of $HClO_4$ could be, at least partially, due to the activation of H_2O_2 with $HClO_4$. Indeed, a blank experiment, without UiO-66 but with the addition of acid in the amount equal to 6 equiv. relative to the basic sites in the catalytic experiment, showed a significant rate of MPS oxidation and predomination of sulfoxide over sulfone (Fig. 8a). From the viewpoint of quantitative measurements, it is important that a clear minimum of activity corresponds to 1 equiv. of acid added. This additionally validates that the liquid-phase adsorption of IBA makes possible reliable and direct determination of the number of basic sites (and, simultaneously, the number of terminal Zr–OH_2/OH pairs).

Acid additives in the amount of 1 equiv. to basic sites also dramatically suppress sulfoxide oxidation to sulfone, which in contrast to the thioether oxidation, becomes negligible upon addition of more acid (Fig. 8b). All the results collectively corroborate that the basicity of the Zr-OH terminal groups does play a key role in the activation of hydrogen peroxide and thioether oxidation to sulfone.

3.6. Role of basic sites in H_2O_2 degradation

Since unproductive degradation of H_2O_2 is the main side reaction in H_2O_2-based oxidations, which may strongly affect the product selectivity and oxidant utilization efficiency, we also studied kinetics of H_2O_2 decay in the presence of UiO-66, with and without the addition of $HClO_4$ to clarify the role of basic sites in the side reaction. Previously, Maksimchuk et al. have found that the addition of 0.1 equiv. of $HClO_4$ per Zr significantly suppressed unproductive H_2O_2 decomposition and strongly enhanced heterolytic pathway in cyclohexene oxidation over UiO-66 and other Zr-MOFs [38,40]. Note that for this sample 0.1 equiv. per Zr corresponds to ca. 0.8 equiv. relative to basic sites.

We have found that, in effect, even smaller amounts of acid (starting from 0.1 equiv. per basic sites) affect the H_2O_2 decomposition kinetics, which has a sigmoidal character (Fig. 9), typical of chain radical processes. The induction period on the kinetic curves of H_2O_2 decay associated with accumulation of radical species (chain initiation) increases with increasing amount of acid (Fig. 9). This dependence of the induction period on the acid amount suggests that basicity of Zr-MOF also plays a significant role in the homolytic H_2O_2 decomposition.

Importantly, the rates of unproductive H_2O_2 decomposition are much lower than the typical rates of MPS oxidation on UiO-66 (especially considering that H_2O_2 decomposition was studied at 50 °C while the thioether oxidations were carried out at 25 °C), which means that the radicals formed during the decomposition of H_2O_2 do not make a significant contribution to the observed catalytic activity. However, the situation may change drastically when less reactive substrates are subjected to oxidation.

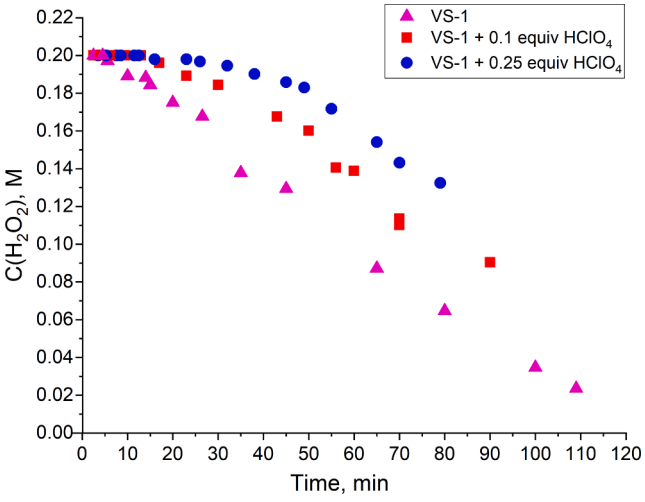

Fig. 9. Effect of acid additives on kinetic curves of H_2O_2 decomposition over UiO-66 (VS-1, 650 μmol/g of basic sites, $HClO_4$ equiv. relative to basic sites). Reaction conditions: 10 mg UiO-66, 0.2 M H_2O_2, 2 mL CH_3CN, 50 °C.

4. Conclusion

In this work we have demonstrated that liquid-phase adsorption of isobutyric acid is a reliable and affordable methodology for direct quantitative determination of basic sites in Zr–MOFs, in particular UiO–66, regardless the number of defects in the sample, particle size and other characteristics. For hydrated UiO-66 samples, the number of basic sites determined by IBA adsorption coincides well with the number of terminal Zr-OH_2/Zr-OH pairs in the open sites of the Zr-MOF defects, which can be assessed using combinations of TGA + ^{1}H NMR and ICP-OES + ^{1}H NMR, among which the former seems to give more consistent results. Therefore, we have found strong evidence in favor of the hypothesis that basic sites in hydrated UiO-66 are represented by terminal Zr-OH groups in defects, which in turn confirms the previously suggested dual acid/base character of the Zr-MOF. The disappearance of the basic sites after dehydration of UiO-66 and reappearance after hydration corroborates their assignment to terminal Zr-OH. In addition, the results of this work demonstrate that adsorption of IBA can be employed for assessment of the number open sites in Zr-MOFs.

Kinetic studies using a range of well-characterized UiO-66 samples differing in the average particle size, total number of defects, and number of open and basic sites have shown that activity of UiO-66 in methyl phenyl sulfide oxidation with H_2O_2 depends linearly on the number of basic sites, provided that the particle size of the MOF does not exceed 10–20 nm. For catalysts with larger particles, diffusion limitations lead to significant reduction of the oxidation rate. Acid additives suppress both the thioether oxidation and H_2O_2 dismutation, pointing to the key role of basic Zr–OH groups in both catalytic reactions.

Declaration of Competing Interest

The authors declare that they have no known competing financial interests or personal relationships that could have appeared to influence the work reported in this paper.

Data availability

Data will be made available on request.

Acknowledgements

The authors thank Dr Danil Kolokolov for fruitful discussions. Help of Dr Igor Soshnikov in measuring ^{1}H NMR spectra is greatly appreciated. The work was supported by RSCF grant № 21-73-00239 https://rscf.ru/en/project/21-73-00239/. The studies were conducted using the equipment of the shared research center "National center of investigation of catalysts" at the Boreskov Institute of Catalysis. The authors also acknowledge the shared resource center "VTAN" (Novosibirsk State University) for the access to TEM equipment.

Appendix A. Supplementary material

Supplementary data to this article can be found online at https://doi.org/10.1016/j.jcat.2023.115099.

References

[1] S.L. James, Metal-organic frameworks, Chem. Soc. Rev. 32 (2003) 276–288, https://doi.org/10.1039/B200393G.
[2] J.L. Rowsell, O.M. Yaghi, Metal–organic frameworks: a new class of porous materials, Microporous Mesoporous Mater. 73 (2004) 3–14, https://doi.org/10.1016/j.micromeso.2004.03.034.
[3] H. Furukawa, K.E. Cordova, M. O'Keeffe, O.M. Yaghi, The chemistry and applications of metal-organic frameworks, Science 341 (2013) 1230444, https://doi.org/10.1126/science.1230444.
[4] O.K. Farha, J.T. Hupp, Rational design, synthesis, purification, and activation of metal−organic framework materials, Acc. Chem. Res. 43 (2010) 1166–1175, https://doi.org/10.1021/ar1000617.
[5] J.R. Li, R.J. Kuppler, H.C. Zhou, Selective gas adsorption and separation in metal–organic frameworks, Chem. Soc. Rev. 38 (2009) 1477–1504, https://doi.org/10.1039/B802426J.
[6] R.B. Lin, S. Xiang, H. Xing, W. Zhou, B. Chen, Exploration of porous metal–organic frameworks for gas separation and purification, Coord. Chem. Rev. 378 (2019) 87–103, https://doi.org/10.1016/j.ccr.2017.09.027.
[7] T. Wang, E. Lin, Y.L. Peng, Y. Chen, P. Cheng, Z. Zhang, Rational design and synthesis of ultramicroporous metal-organic frameworks for gas separation, Coord. Chem. Rev. 423 (2020), 213485, https://doi.org/10.1016/j.ccr.2020.213485.
[8] S.K. Henninger, H.A. Habib, C. Janiak, MOFs as adsorbents for low temperature heating and cooling applications, J. Am. Chem. Soc. 131 (2009) 2776–2777, https://doi.org/10.1021/ja808444z.
[9] S.K. Henninger, F. Jeremias, H. Kummer, C. Janiak, MOFs for use in adsorption heat pump processes, Eur. J. Inorg. Chem. 2012 (2012) 2625–2634, https://doi.org/10.1002/ejic.201101056.
[10] J. Lee, O.K. Farha, J. Roberts, K.A. Scheidt, S.T. Nguyen, J.T. Hupp, Metal–organic framework materials as catalysts, Chem. Soc. Rev. 38 (2009) 1450–1459, https://doi.org/10.1039/B807080F.
[11] J. Gascon, A. Corma, F. Kapteijn, F.X. Llabres i Xamena, Metal organic framework catalysis: Quo vadis? ACS Catal. 4 (2014) 361–378, https://doi.org/10.1021/cs400959k.
[12] P. García-García, M. Müller, A. Corma, MOF catalysis in relation to their homogeneous counterparts and conventional solid catalysts, Chem. Sci. 5 (2014) 2979–3007, https://doi.org/10.1039/C4SC00265B.
[13] Q. Wang, D. Astruc, State of the art and prospects in metal–organic framework (MOF)-based and MOF-derived nanocatalysis, Chem. Rev. 120 (2019) 1438–1511, https://doi.org/10.1021/acs.chemrev.9b00223.
[14] D. Yang, B.C. Gates, Catalysis by metal organic frameworks: perspective and suggestions for future research, ACS Catal. 9 (2019) 1779–1798, https://doi.org/10.1021/acscatal.8b04515.
[15] A. Bavykina, N. Kolobov, I.S. Khan, J.A. Bau, A. Ramirez, J. Gascon, Metal–organic frameworks in heterogeneous catalysis: recent progress, new trends, and future perspectives, Chem. Rev. 120 (2020) 8468–8535, https://doi.org/10.1021/acs.chemrev.9b00685.
[16] E.A. Dolgopolova, A.M. Rice, C.R. Martin, N.B. Shustova, Photochemistry and photophysics of MOFs: steps towards MOF-based sensing enhancements, Chem. Soc. Rev. 47 (2018) 4710–4728, https://doi.org/10.1039/C7CS00861A.
[17] C. He, D. Liu, W. Lin, Nanomedicine applications of hybrid nanomaterials built from metal–ligand coordination bonds: nanoscale metal–organic frameworks and nanoscale coordination polymers, Chem. Rev. 115 (2015) 11079–11108, https://doi.org/10.1021/acs.chemrev.5b00125.
[18] M.X. Wu, Y.W. Yang, Metal–organic framework (MOF)-based drug/cargo delivery and cancer therapy, Adv. Mater. 29 (2017) 1606134, https://doi.org/10.1002/adma.201606134.
[19] Y.K. Hwang, G. Férey, U.-H. Lee, J.-S. Chang, Liquid phase oxidation of organic compounds by metal-organic frameworks, in: M.G. Clerici, O.A. Kholdeeva (Eds.), Liquid Phase Oxidation Via Heterogeneous Catalysis: Organic Synthesis and Industrial Applications, Wiley, Hoboken, NJ, USA, 2013, pp. 371–409, https://doi.org/10.1002/9781118356760.ch8.
[20] P. Valvekens, F. Vermoortele, D. De Vos, Metal–organic frameworks as catalysts: The role of metal active sites, Catal. Sci. Technol. 3 (2013) 1435–1445, https://doi.org/10.1039/C3CY20813C.
[21] A. Dhakshinamoorthy, A.M. Asiri, H. García, Metal–organic frameworks as catalysts for oxidation reactions, Chem Eur J 22 (2016) 8012–8024, https://doi.org/10.1002/chem.201505141.
[22] T. Drake, P. Ji, W. Lin, Site isolation in metal–organic frameworks enables novel transition metal catalysis, Acc. Chem. Res. 51 (2018) 2129–2138, https://doi.org/10.1021/acs.accounts.8b00297.
[23] R.A. Sheldon, I.W.C.E. Arends, U. Hanefeld, Green chemistry and catalysis, Wiley VCH, Weinheim, Germany (2007), https://doi.org/10.1002/9783527611003.
[24] M.G. Clerici, O.A. Kholdeeva (Eds.), Liquid Phase Oxidation Via Heterogeneous Catalysis: Organic Synthesis and Industrial Applications, Wiley, Hoboken, NJ, USA, 2013.
[25] D. Duprez, F. Cavani (Eds.), Handbook of Advanced Methods and Processes in Oxidation Catalysis: From Laboratory to Industry, Imperial Press, London, UK, 2014, https://doi.org/10.1142/p791.
[26] G. Strukul, A. Scarso, Environmentally benign oxidants, in: M.G. Clerici, O. A. Kholdeeva (Eds.), Liquid Phase Oxidation Via Heterogeneous Catalysis: Organic Synthesis and Industrial Applications, Wiley, Hoboken, NJ, USA, 2013, pp. 1–20, https://doi.org/10.1002/9781118356760.ch1.
[27] A. Goti, F. Cardona, Hydrogen peroxide in green oxidation reactions: recent catalytic processes, in: P. Tundo, V. Esposito (Eds.), Green Chemical Reactions, Springer, Dordrecht, 2008, pp. 191–212, https://doi.org/10.1007/978-1-4020-8457-7_9.
[28] F. Menegazzo, M. Signoretto, E. Ghedini, G. Strukul, Looking for the "dream catalyst" for hydrogen peroxide production from hydrogen and oxygen, Catalysts 9 (2019) 251, https://doi.org/10.3390/catal9030251.
[29] O.A. Kholdeeva, N.V. Maksimchuk, Metal-organic frameworks in oxidation catalysis with hydrogen peroxide, Catalysts 11 (2021) 283, https://doi.org/10.3390/catal11020283.
[30] A.J. Howarth, Y. Liu, P. Li, Z. Li, T.C. Wang, J.T. Hupp, O.K. Farha, Chemical, thermal and mechanical stabilities of metal–organic frameworks, Nat. Rev. Mater. 1 (2016) 1–15, https://doi.org/10.1038/natrevmats.2015.18.
[31] J.H. Cavka, S. Jakobsen, U. Olsbye, N. Guillou, C. Lamberti, S. Bordiga, K. P. Lillerud, A new zirconium inorganic building brick forming metal organic frameworks with exceptional stability, J. Am. Chem. Soc. 130 (2008) 13850–13851, https://doi.org/10.1021/ja8057953.
[32] J. Winarta, B. Shan, S.M. Mcintyre, L. Ye, C. Wang, J. Liu, B. Mu, A decade of UiO-66 research: a historic review of dynamic structure, synthesis mechanisms, and characterization techniques of an archetypal metal–organic framework, Cryst. Growth Des. 20 (2019) 1347–1362, https://doi.org/10.1021/acs.cgd.9b00955.
[33] Y. Bai, Y. Dou, L.H. Xie, W. Rutledge, J.R. Li, H.C. Zhou, Zr-based metal–organic frameworks: design, synthesis, structure, and applications, Chem. Soc. Rev. 45 (2016) 2327–2367, https://doi.org/10.1039/C5CS00837A.
[34] X. Zhang, F. Bi, Z. Zhao, Y. Yang, Y. Li, L. Song, N. Liu, J. Xu, L. Cui, Boosting toluene oxidation by the regulation of Pd species on UiO-66: Synergistic effect of Pd species, J. Catal. 413 (2022) 59–75, https://doi.org/10.1016/j.jcat.2022.06.015.
[35] D. de la Flor, C. Lopez-Aguado, M. Paniagua, G. Morales, R. Mariscal, J.A. Melero, Defective UiO-66 (Zr) as an efficient catalyst for the synthesis of bio jet-fuel precursors via aldol condensation of furfural and MIBK, J. Catal. 401 (2021) 27–39, https://doi.org/10.1016/j.jcat.2021.07.006.
[36] L. Zou, M. Chen, Q. Zhang, Q. Mao, Y. Huang, Z. Liang, Pd/UIO-66/sepiolite: Toward highly efficient dual-supported Pd-based catalyst for dehydrogenation of formic acid at room temperature, J. Catal. 388 (2020) 66–76, https://doi.org/10.1016/j.jcat.2020.05.010.
[37] A. Santiago-Portillo, S. Navalón, M. Álvaro, H. García, Generating and optimizing the catalytic activity in UiO-66 for aerobic oxidation of alkenes by post-synthetic exchange Ti atoms combined with ligand substitution, J. Catal. 365 (2018) 450–463, https://doi.org/10.1016/j.jcat.2018.07.032.

[38] N.V. Maksimchuk, J.S. Lee, M.V. Solovyeva, K.H. Cho, A.N. Shmakov, Y. A. Chesalov, J.-S. Chang, O.A. Kholdeeva, Protons make possible heterolytic activation of hydrogen peroxide over Zr-based metal–organic frameworks, ACS Catal. 9 (2019) 9699–9704, https://doi.org/10.1021/acscatal.9b02941.

[39] O.V. Zalomaeva, V.Y. Evtushok, I.D. Ivanchikova, T.S. Glazneva, Y.A. Chesalov, K.P. Larionov, I.Y. Skobelev, O.A. Kholdeeva, Nucleophilic versus Electrophilic Activation of Hydrogen Peroxide over Zr-Based Metal-Organic Frameworks, Inorg. Chem. 59 (2020) 10634–10649, https://doi.org/10.1021/acs.inorgchem.0c01084.

[40] N.V. Maksimchuk, I.D. Ivanchikova, K.H. Cho, O.V. Zalomaeva, V.Y. Evtushok, K. P. Larionov, T.S. Glazneva, J.-S. Chang, O.A. Kholdeeva, Catalytic Performance of Zr-Based Metal-Organic Frameworks Zr-abtc and MIP-200 in Selective Oxidations with H2O2, Chem Eur J 27 (2021) 6985–6992, https://doi.org/10.1002/chem.202005152.

[41] V.V. Torbina, N.S. Nedoseykina, I.D. Ivanchikova, O.A. Kholdeeva, O. V. Vodyankina, Propylene glycol oxidation with hydrogen peroxide over Zr-containing metal-organic framework UiO-66, Catal. Today 333 (2019) 47–53, https://doi.org/10.1016/j.cattod.2018.11.063.

[42] L. Hao, S.A. Stoian, L.R. Weddle, Q. Zhang, Zr-Based MOFs for oxidative desulfurization: what matters? Green Chem. 22 (2020) 6351–6356, https://doi.org/10.1039/D0GC01999B.

[43] B.N. Bhadra, S.H. Jhung, Oxidative desulfurization and denitrogenation of fuels using metal-organic framework-based/-derived catalysts, Appl. Catal. B Environ. 118021 (2019) 259, https://doi.org/10.1016/j.apcatb.2019.118021.

[44] C. Vallés-García, A. Santiago-Portillo, M. Álvaro, S. Navalon, H. Garcia, MIL-101 (Cr)-NO2 as efficient catalyst for the aerobic oxidation of thiophenols and the oxidative desulfurization of dibenzothiophenes, Appl. Catal. A 590 (2020), 117340, https://doi.org/10.1016/j.apcata.2019.117340.

[45] X. Zhang, P. Huang, A. Liu, M. Zhu, A metal–organic framework for oxidative desulfurization: UiO-66 (Zr) as a catalyst, Fuel 209 (2017) 417–423, https://doi.org/10.1016/j.fuel.2017.08.025.

[46] C.M. Granadeiro, S.O. Ribeiro, M. Karmaoui, R. Valença, J.C. Ribeiro, B. de Castro, L. Cunha-Silva, S.S. Balula, Production of ultra-deep sulfur-free diesels using a sustainable catalytic system based on UiO-66 (Zr), Chem. Comm. 51 (2015) 13818–13821, https://doi.org/10.1039/C5CC03958D.

[47] G. Ye, D. Zhang, X. Li, K. Leng, W. Zhang, J. Ma, Y. Sun, W. Xu, S. Ma, Boosting catalytic performance of metal–organic framework by increasing the defects via a facile and green approach, ACS Appl. Mater. Interfaces 9 (2017) 34937–34943, https://doi.org/10.1021/acsami.7b10337.

[48] W. Xiao, Q. Dong, Y. Wang, Y. Li, S. Deng, N. Zhang, Time modulation of defects in UiO-66 and application in oxidative desulfurization, CrystEngComm 20 (2018) 5658–5662, https://doi.org/10.1039/C8CE00795K.

[49] G. Ye, H. Qi, W. Zhou, W. Xu, Y. Sun, Green and scalable synthesis of nitro-and amino-functionalized UiO-66 (Zr) and the effect of functional groups on the oxidative desulfurization performance, Inorg. Chem. Front. 6 (2019) 1267–1274, https://doi.org/10.1039/C9QI00172G.

[50] A.M. Viana, S.O. Ribeiro, B.D. Castro, S.S. Balula, L. Cunha-Silva, Influence of UiO-66 (Zr) preparation strategies in its catalytic efficiency for desulfurization process, Materials 12 (2019) 3009, https://doi.org/10.3390/ma12183009.

[51] H.Q. Zheng, Y.N. Zeng, J. Chen, R.G. Lin, W.E. Zhuang, R. Cao, Z.J. Lin, Zr-based metal–organic frameworks with intrinsic peroxidase-like activity for ultradeep oxidative desulfurization: mechanism of H_2O_2 decomposition, Inorg. Chem. 58 (2019) 6983–6992, https://doi.org/10.1021/acs.inorgchem.9b00604.

[52] R. Limvorapitux, H. Chen, M.L. Mendonca, M. Liu, R.Q. Snurr, S.T. Nguyen, Elucidating the mechanism of the UiO-66-catalyzed sulfide oxidation: activity and selectivity enhancements through changes in the node coordination environment and solvent, Catal. Sci. Technol. 9 (2019) 327–335, https://doi.org/10.1039/C8CY01139G.

[53] G. Ye, H. Wang, X. Zeng, L. Wang, J. Wang, Defect-rich bimetallic UiO-66 (Hf-Zr): Solvent-free rapid synthesis and robust ambient-temperature oxidative desulfurization performance, Appl. Catal. B Environ. 299 (2021), 120659, https://doi.org/10.1016/j.apcatb.2021.120659.

[54] H.G.T. Nguyen, L. Mao, A.W. Peters, C.O. Audu, Z.J. Brown, O.K. Farha, J. T. Hupp, S.T. Nguyen, Comparative study of titanium-functionalized UiO-66: support effect on the oxidation of cyclohexene using hydrogen peroxide, Catal. Sci. Technol. 5 (2015) 4444–4451, https://doi.org/10.1039/C5CY00825E.

[55] S. Ahn, N.E. Thornburg, Z. Li, T.C. Wang, L.C. Gallington, K.W. Chapman, J. M. Notestein, J.T. Hupp, O.K. Farha, Stable metal–organic framework-supported niobium catalysts, Inorg. Chem. 55 (2016) 11954–11961, https://doi.org/10.1021/acs.inorgchem.6b02103.

[56] N.V. Maksimchuk, V.Y. Evtushok, O.V. Zalomaeva, G.M. Maksimov, I. D. Ivanchikova, Y.A. Chesalov, I.V. Eltsov, P.A. Abramov, T.S. Glazneva, V. V. Yanshole, O.A. Kholdeeva, R.J. Errington, A. Solé-Daura, J.M. Poblet, J. J. Carbó, Activation of H2O2 over Zr (IV), Insights from model studies on Zr-monosubstituted Lindqvist tungstates, ACS Catal. 11 (2021) 10589–10603, https://doi.org/10.1021/acscatal.1c02485.

[57] I.D. Ivanchikova, O.V. Zalomaeva, N.V. Maksimchuk, O.A. Stonkus, T. S. Glazneva, Y.A. Chesalov, A.N. Shmakov, M. Guidotti, O.A. Kholdeeva, Alkene Epoxidation and Thioether Oxidation with Hydrogen Peroxide Catalyzed by Mesoporous Zirconium-Silicates, Catalysts 12 (2022) 742, https://doi.org/10.3390/catal12070742.

[58] X. Feng, H.S. Jena, C. Krishnaraj, K. Leus, G. Wang, H. Chen, C. Jia, P. Van Der Voort, Generating Catalytic Sites in UiO-66 through Defect Engineering, ACS Appl. Mater. Interfaces 13 (2021) 60715–60735, https://doi.org/10.1021/acsami.1c13525.

[59] P. Gairola, Y. Millot, J.M. Krafft, F. Averseng, F. Launay, P. Massiani, C. Jolivalt, J. Reboul, On the importance of combining bulk-and surface-active sites to maximize the catalytic activity of metal–organic frameworks for the oxidative dehydrogenation of alcohols using alkyl hydroperoxides as hydride acceptors,, Catal. Sci. Technol. 10 (2020) 6935–6947, https://doi.org/10.1039/D0CY00901F.

[60] A. Dhakshinamoorthy, A. Santiago-Portillo, A.M. Asiri, H. Garcia, Engineering UiO-66 metal organic framework for heterogeneous catalysis, ChemCatChem 11 (2019) 899–923, https://doi.org/10.1002/cctc.201801452.

[61] F. Faccioli, M. Bauer, D. Pedron, A. Sorarù, M. Carraro, S. Gross, Hydrolytic Stability and Hydrogen Peroxide Activation of Zirconium-Based Oxoclusters, Eur. J. Inorg. Chem. 2015 (2015) 210–225, https://doi.org/10.1002/ejic.201402767.

[62] Y. Feng, Q. Chen, M. Jiang, J. Yao, Tailoring the properties of UiO-66 through defect engineering: A review, Ind. Eng. Chem. Res. 58 (2019) 17646–17659, https://doi.org/10.1021/acs.iecr.9b03188.

[63] J. Jiang, O.M. Yaghi, Brønsted acidity in metal–organic frameworks, Chem. Rev. 115 (2015) 6966–6997, https://doi.org/10.1021/acs.chemrev.5b00221.

[64] S. Ling, B. Slater, Dynamic acidity in defective UiO-66, Chem. Sci. 7 (2016) 4706–4712, https://doi.org/10.1039/C5SC04953A.

[65] C. Caratelli, J. Hajek, F.G. Cirujano, M. Waroquier, F.X.L. i Xamena, V. Van Speybroeck, Nature of active sites on UiO-66 and beneficial influence of water in the catalysis of Fischer esterification, J. Catal. 352 (2017) 401-414, doi:10.1016/j.jcat.2017.06.014.

[66] D. Yang, V. Bernales, T. Islamoglu, O.K. Farha, J.T. Hupp, C.J. Cramer, B.C. Gates, Tuning the surface chemistry of metal organic framework nodes: proton topology of the metal-oxide-like Zr6 nodes of UiO-66 and NU-1000, J. Am. Chem. Soc. 138 (2016) 15189–15196, https://doi.org/10.1021/jacs.6b08273.

[67] M. Taddei, When defects turn into virtues: The curious case of zirconium-based metal-organic frameworks, Coord. Chem. Rev. 343 (2017) 1–24, https://doi.org/10.1016/j.ccr.2017.04.010.

[68] F. Vermoortele, B. Bueken, G. Le Bars, B. Van de Voorde, M. Vandichel, K. Houthoofd, A. Vimont, M. Daturi, M. Waroquier, V. Van Speybroeck, C. Kirschhock, D. De Vos, Synthesis modulation as a tool to increase the catalytic activity of metal–organic frameworks: the unique case of UiO-66 (Zr), J. Am. Chem. Soc. 135 (2013) 11465–11468, https://doi.org/10.1021/ja405078u.

[69] G.C. Shearer, S. Chavan, S. Bordiga, S. Svelle, U. Olsbye, K.P. Lillerud, Defect engineering: tuning the porosity and composition of the metal–organic framework UiO-66 via modulated synthesis, Chem. Mater. 28 (2016) 3749–3761, https://doi.org/10.1021/acs.chemmater.6b00602.

[70] W. Liang, C.J. Coghlan, F. Ragon, M. Rubio-Martinez, D.M. D'Alessandro, R. Babarao, Defect engineering of UiO-66 for CO_2 and H_2O uptake–a combined experimental and simulation study, Dalton Trans. 45 (2016) 4496–4500, https://doi.org/10.1039/C6DT00189K.

[71] F.G. Cirujano, F.x., Llabrés i Xamena, Tuning the Catalytic Properties of UiO-66 Metal-Organic Frameworks: From Lewis to Defect-Induced Brønsted Acidity, J. Phys. Chem. Lett. 11 (2020) 4879–4890, https://doi.org/10.1021/acs.jpclett.0c00984.

[72] C. Caratelli, J. Hajek, S.M. Rogge, S. Vandenbrande, E.J. Meijer, M. Waroquier, V. Van Speybroeck, Influence of a Confined Methanol Solvent on the Reactivity of Active Sites in UiO-66, ChemPhysChem 19 (2018) 420–429, https://doi.org/10.1002/cphc.201701109.

[73] F. Di Furia, G. Modena, Mechanism of oxygen transfer from peroxo species, Pure Appl. Chem. 54 (1982) 1853–1866, https://doi.org/10.1351/pac198254101853.

[74] M.V. Gómez, R. Caballero, E. Vazquez, A. Moreno, A. de la Hoz, A. Diaz-Ortiz, Green and chemoselective oxidation of sulfides with sodium perborate and sodium percarbonate: nucleophilic and electrophilic character of the oxidation system, Green Chem. 9 (2007) 331–336, https://doi.org/10.1039/B614847F.

[75] R. Curci, A. Giovine, G. Modena, Oxidation of organic sulphides—XVI: Rate of alkaline and acidic oxidation of p-tolyl methyl sulphoside with substituted peroxybenzoic acids, Tetrahedron 22 (1966) 1235–1239, https://doi.org/10.1016/S0040-4020(01)99415-3.

[76] D.E. Richardson, H. Yao, K.M. Frank, D.A. Bennett, Equilibria, kinetics, and mechanism in the bicarbonate activation of hydrogen peroxide: oxidation of sulfides by peroxymonocarbonate, J. Am. Chem. Soc. 122 (2000) 1729–1739, https://doi.org/10.1021/ja9927467.

[77] J. Hajek, B. Bueken, M. Waroquier, D. De Vos, V. Van Speybroeck, The Remarkable Amphoteric Nature of Defective UiO-66 in Catalytic Reactions, ChemCatChem 9 (2017) 2203–2210, https://doi.org/10.1002/cctc.201601689.

[78] E. Plessers, D. De Vos, M.B. Roeffaers, Chemoselective reduction of α, β-unsaturated carbonyl compounds with UiO-66 materials, J. Catal. 340 (2016) 136–143, https://doi.org/10.1016/j.jcat.2016.05.013.

[79] K. Chakarova, I. Strauss, M. Mihaylov, N. Drenchev, K. Hadjiivanov, Evolution of acid and basic sites in UiO-66 and UiO-66-NH2 metal-organic frameworks: FTIR study by probe molecules, Microporous Mesoporous Mater. 281 (2019) 110–122, https://doi.org/10.1016/j.micromeso.2019.03.006.

[80] H. Wu, Y.S. Chua, V. Krungleviciute, M. Tyagi, P. Chen, T. Yildirim, W. Zhou, Unusual and highly tunable missing-linker defects in zirconium metal–organic framework UiO-66 and their important effects on gas adsorption, J. Am. Chem. Soc. 135 (2013) 10525–10532, https://doi.org/10.1021/ja404514r.

[81] M.I. Hossain, J.D. Cunningham, T.M. Becker, B.E. Grabicka, K.S. Walton, B. D. Rabideau, T.G. Glover, Impact of MOF defects on the binary adsorption of CO2 and water in UiO-66, Chem. Eng. Sci. 203 (2019) 346–357, https://doi.org/10.1016/j.ces.2019.03.053.

[82] X. Shi, X. Zhang, F. Bi, Z. Zheng, L. Sheng, J. Xu, Z. Wang, Y. Yang, Effective toluene adsorption over defective UiO-66-NH2: An experimental and

computational exploration, J. Mol. Liq. 316 (2020), 113812, https://doi.org/10.1016/j.molliq.2020.113812.
[83] S. Ali, Z. Zuhra, Y. Abbas, Y. Shu, M. Ahmad, Z. Wang, Tailoring defect density in UiO-66 frameworks for enhanced Pb (II) adsorption, Langmuir 37 (2021) 13602–13609, https://doi.org/10.1021/acs.langmuir.1c02032.
[84] H.G.T. Ly, G. Fu, A. Kondinski, B. Bueken, D. De Vos, T.N. Parac-Vogt, Superactivity of MOF-808 toward peptide bond hydrolysis, J. Am. Chem. Soc. 140 (2018) 6325–6335, https://doi.org/10.1021/jacs.8b01902.
[85] M. Sarker, J.Y. Song, S.H. Jhung, Carboxylic-acid-functionalized UiO-66-NH2: a promising adsorbent for both aqueous-and non-aqueous-phase adsorptions, J. Chem. Eng. 331 (2018) 124–131, https://doi.org/10.1016/j.cej.2017.08.017.
[86] M.A. Moreira, J.C. Santos, A.F. Ferreira, J.M. Loureiro, F. Ragon, P. Horcajada, K.-E. Shim, Y.-K. Hwang, U.-H. Lee, J.-S. Chang, C. Serre, A.E. Rodrigues, Reverse shape selectivity in the liquid-phase adsorption of xylene isomers in zirconium terephthalate MOF UiO-66, Langmuir 28 (2012) 5715–5723, https://doi.org/10.1021/la3004118.
[87] Q. He, Q. Chen, M. Lü, X. Liu, Adsorption behavior of rhodamine B on UiO-66, Chin. J. Chem. Eng. 22 (2014) 1285–1290, https://doi.org/10.1016/j.cjche.2014.09.009.
[88] D.V. Brazhnik, I.Y. Skobelev, K.A. Kovalenko, O.A. Kholdeeva, Quantitative analysis of liquid-phase adsorption over chromium-containing metal–organic frameworks of MTN topology, Adsorption (2021) 1–10, https://doi.org/10.1007/s10450-020-00287-4.
[89] M.I. Hossain, T.G. Glover, Kinetics of water adsorption in UiO-66 MOF, Ind. Eng. Chem. Res. 58 (2019) 10550–10558, https://doi.org/10.1021/acs.iecr.9b00976.
[90] N.A. Ramsahye, J. Gao, H. Jobic, P.L. Llewellyn, Q. Yang, A.D. Wiersum, M. M. Koza, V. Guillerm, C. Serre, C.L. Zhong, G. Maurin, Adsorption and diffusion of light hydrocarbons in UiO-66 (Zr): a combination of experimental and modeling tools, J. Phys. Chem. C 118 (2014) 27470–27482, https://doi.org/10.1021/jp509672c.
[91] C.H. Sharp, J. Abelard, A.M. Plonka, W. Guo, C.L. Hill, J.R. Morris, Alkane–OH hydrogen bond formation and diffusion energetics of n-butane within UiO-66, J. Phys. Chem. C 121 (2017) 8902–8906, https://doi.org/10.1021/acs.jpcc.7b01351.
[92] Q. Yang, H. Jobic, F. Salles, D. Kolokolov, V. Guillerm, C. Serre, G. Maurin, Probing the Dynamics of CO2 and CH4 within the Porous Zirconium Terephthalate UiO-66 (Zr): A Synergic Combination of Neutron Scattering Measurements and Molecular Simulations, Chem Eur J 17 (2011) 8882–8889, https://doi.org/10.1002/chem.201003596.
[93] X. Zhang, Y. Yang, X. Lv, Y. Wang, N. Liu, D. Chen, L. Cui, Adsorption/desorption kinetics and breakthrough of gaseous toluene for modified microporous-mesoporous UiO-66 metal organic framework, J. Hazard. Mater. 366 (2019) 140–150, https://doi.org/10.1016/j.jhazmat.2018.11.099.
[94] S. Wang, M.C. Oliver, Y. An, E. Chen, Z. Su, A. Kleinhammes, Y. Wu, L. Huang, A Computational Study of Isopropyl Alcohol Adsorption and Diffusion in UiO-66 Metal-Organic Framework: The Role of Missing Linker Defect, J. Phys. Chem. B 125 (2021) 3690–3699, https://doi.org/10.1021/acs.jpcb.0c11252.
[95] C.N. Satterfield, Mass transfer in heterogeneous catalysis, MIT press (1970).
[96] M. Taddei, K.C. Dümbgen, J.A. van Bokhoven, M. Ranocchiari, Aging of the reaction mixture as a tool to modulate the crystallite size of UiO-66 into the low nanometer range, Chem. Comm. 52 (2016) 6411–6414, https://doi.org/10.1039/C6CC02517J.
[97] O.V. Gutov, M.G. Hevia, E.C. Escudero-Adan, A. Shafir, Metal–organic framework (MOF) defects under control: insights into the missing linker sites and their implication in the reactivity of zirconium-based frameworks, Inorg. Chem. 54 (2015) 8396–8400, https://doi.org/10.1021/acs.inorgchem.5b01053.
[98] P. Carniti, A. Gervasini, C. Tiozzo, M. Guidotti, Niobium-containing hydroxyapatites as amphoteric catalysts: synthesis, properties, and activity, ACS Catal. 4 (2014) 469–479, https://doi.org/10.1021/cs4010453.
[99] J.I. Langford, A.J.C. Wilson, Scherrer after sixty years: a survey and some new results in the determination of crystallite size, J. Appl. Cryst. 11 (1978) 102–113, https://doi.org/10.1107/S0021889878012844.
[100] C. Atzori, G.C. Shearer, L. Maschio, B. Civalleri, F. Bonino, C. Lamberti, S. Svelle, K.P. Lillerud, S. Bordiga, Effect of benzoic acid as a modulator in the structure of UiO-66: an experimental and computational study, J. Phys. Chem. C 121 (2017) 9312–9324, https://doi.org/10.1021/acs.jpcc.7b00483.
[101] D.M. Driscoll, D. Troya, P.M. Usov, A.J. Maynes, A.J. Morris, J.R. Morris, Characterization of undercoordinated Zr defect sites in UiO-66 with vibrational spectroscopy of adsorbed CO, J. Phys. Chem. C 122 (2018) 14582–14589, https://doi.org/10.1021/acs.jpcc.8b03283.
[102] J. Yin, Z. Kang, Y. Fu, W. Cao, Y. Wang, H. Guan, X. Kong, Molecular identification and quantification of defect sites in metal-organic frameworks with NMR probe molecules, Nat. Comm. 13 (2022) 1–9, https://doi.org/10.1038/s41467-022-32809-9.
[103] W.L. Peng, F. Liu, X. Yi, S. Sun, H. Shi, Y. Hui, A. Zheng, Structural and Acidic Characteristics of Multiple Zr Defect Sites in UiO-66 Metal-Organic Frameworks, J. Phys. Chem. Lett. 13 (2022) 9295–9302, https://doi.org/10.1021/acs.jpclett.2c02468.
[104] Y. Liu, R.C. Klet, J.T. Hupp, O. Farha, Probing the Correlations between the Defects in Metal-Organic Frameworks and Their Catalytic Activity by an Epoxide Ring-Opening Reaction, Chem. Commun. 52 (2016) 7806–7809, https://doi.org/10.1039/C6CC03727E.
[105] R.C. Klet, Y. Liu, T.C. Wang, J.T. Hupp, O.K. Farha, Evaluation of Brønsted Acidity and Proton Topology in Zr- and Hf-Based Metal-Organic Frameworks Using Potentiometric Acid-Base Titration, J. Mater. Chem. A 4 (2016) 1479–1485, https://doi.org/10.1039/C5TA07687K.
[106] G.C. Shearer, S. Chavan, J. Ethiraj, J.G. Vitillo, S. Svelle, U. Olsbye, C. Lamberti, S. Bordiga, K.P. Lillerud, Tuned to perfection: ironing out the defects in metal–organic framework UiO-66, Chem. Mater. 26 (2014) 4068–4071, https://doi.org/10.1021/cm501859p.
[107] D.K. Sannes, S. Øien-Ødegaard, E. Aunan, A. Nova, U. Olsbye, Quantification of Linker Defects in UiO-Type Metal-Organic Frameworks, Chem. Mater. 35 (2023) 3793–3800, https://doi.org/10.1021/acs.chemmater.2c03744.
[108] M. Ayranov, J. Cobos, K. Popa, V.V. Rondinella, Determination of REE, U, Th, Ba, and Zr in simulated hydrogeological leachates by ICP-AES after matrix solvent extraction, J. Rare Earths 27 (2009) 123–127, https://doi.org/10.1016/S1002-0721(08)60205-7.
[109] A.D. Wiersum, E. Soubeyrand-Lenoir, Q. Yang, B. Moulin, V. Guillerm, M. B. Yahia, P.L. Llewellyn, An evaluation of UiO-66 for gas-based applications, Chem. Asian J. 6 (2011) 3270–3280, https://doi.org/10.1002/asia.201100201.
[110] M. Vandichel, J. Hajek, A. Ghysels, A. De Vos, M. Waroquier, V. Van Speybroeck, Water coordination and dehydration processes in defective UiO-66 type metal organic frameworks, CrystEngComm 18 (2016) 7056–7069, https://doi.org/10.1039/C6CE01027J.
[111] X. Tang, Y. Luo, Z. Zhang, W. Ding, D. Liu, J. Wang, M. Wen, Effects of functional groups of–NH2 and–NO2 on water adsorption ability of Zr-based MOFs (UiO-66), Chem. Phys. 543 (2021), 111093, https://doi.org/10.1016/j.chemphys.2021.111093.
[112] M.I. Hossain, T.G. Glover, Kinetics of water adsorption in UiO-66 MOF, Ind. Eng. Chem. Res. 58 (24) (2019) 10550–10558, https://doi.org/10.1021/acs.iecr.9b00976.
[113] O.A. Kholdeeva, I.D. Ivanchikova, N.V. Maksimchuk, I.Y. Skobelev, H2O2-based selective epoxidations: Nb-silicates versus Ti-silicates, Catal. Today 333 (2019) 63–70, https://doi.org/10.1016/j.cattod.2018.04.002.
[114] P. Jimenez-Lozano, I.Y. Skobelev, O.A. Kholdeeva, J.M. Poblet, J.J. Carbo, Alkene epoxidation catalyzed by Ti-containing polyoxometalates: unprecedented β-oxygen transfer mechanism, Inorg. Chem. 55 (2016) 6080–6084, https://doi.org/10.1021/acs.inorgchem.6b00621.
[115] D.I. Kolokolov, A.G. Maryasov, J. Ollivier, D. Freude, J. Haase, A.G. Stepanov, H. Jobic, Uncovering the rotation and translational mobility of benzene confined in UiO-66 (Zr) metal–organic framework by the 2H NMR–QENS experimental toolbox, J. Phys. Chem. C 121 (2017) 2844–2857, https://doi.org/10.1021/acs.jpcc.6b12001.
[116] A.E. Khudozhitkov, S.S. Arzumanov, D.I. Kolokolov, A.G. Stepanov, UiO-66 (Zr) MOF as a Promising Material for Butane Isomers Separation: Evidence Based on the Analysis of the Adsorbed Alkanes Mobility by 2H NMR and Molecular Dynamics Simulation, J. Phys. Chem. C 125 (2021) 13391–13400, https://doi.org/10.1021/acs.jpcc.1c02849.